

卤氢键桥联的铁(III)配合物呈现出高于室温的自旋交叉行为

卫晓琴¹ 高转¹ 任帆¹ 崔晓友¹ 周悦² 邵东^{*2,3}

(¹晋中学院材料科学与工程系,山西省轻质材料改性应用协同创新中心,晋中 030619)

(²黄冈师范学院化学化工学院,催化材料制备及应用湖北省重点实验室,黄冈 438000)

(³南京大学配位化学国家重点实验室,南京 210023)

摘要: 使用一个三齿配体2,6-二(苯并咪唑-2-基)吡啶(bzimpy)与三价铁离子反应,制备了一例单核的铁(III)配合物[Fe^{III}(bzimpy-1H)₂]Cl (**1**)(bzimpy-1H为bzimpy脱去一个质子后的产物),并对其结构和磁性质进行了详细表征。单晶结构分析表明配合物中Fe(III)中心处于畸变的N₆八面体配位环境,相邻的阳离子配合物基元与抗衡氯离子通过N—H…Cl氢键作用构建了超分子的三维结构。磁性研究和差示扫描量热法研究表明,配合物表现出高于室温的磁滞自旋交叉(SCO)行为($T_{1/2} \uparrow = 345$ K, $T_{1/2} \downarrow = 330$ K)并且观察到低温光诱导激发自旋态捕获(LIESST)效应。磁构关系研究表明,氯氢键对配合物的双稳态SCO行为具有重要的作用。

关键词: 自旋交叉; 铁配合物; 双稳态; 氢键; 超分子作用

中图分类号: O614.81⁺1 文献标识码: A 文章编号: 1001-4861(2022)11-2283-08

DOI: 10.11862/CJIC.2022.235

A Halogen Hydrogen-Bonded Fe(III) Complex Showing Hysteretic Spin-Crossover Behavior above Room Temperature

WEI Xiao-Qin¹ GAO Zhuan¹ REN Fan¹ CUI Xiao-You¹ ZHOU Yue² SHAO Dong^{*2,3}

(¹Shanxi Province Collaborative Innovation Center for Light Materials Modification and Application, Department of Material Science and Engineering, Jinzhong University, Jinzhong, Shanxi 030619, China)

(²Hubei Key Laboratory of Processing and Application of Catalytic Materials, College of Chemistry and Chemical Engineering, Huanggang Normal University, Huanggang, Hubei 438000, China)

(³State Key Laboratory of Coordination Chemistry, Nanjing University, Nanjing 210023, China)

Abstract: A mononuclear Fe(III) complex, [Fe^{III}(bzimpy-1H)₂]Cl (**1**) was prepared by the reaction of a tridentate ligand 2,6-bis(benzimidazol-2-yl)pyridine (bzimpy), where bzimpy-1H is the product of bzimpy after removing one proton, and its structure and magnetic properties were characterized in detail. The single crystal structure analysis shows that the Fe³⁺ center features a rare distorted octahedral N₆ coordination environment for the complex, and the 3D supramolecular structure is constructed by N—H…Cl hydrogen bonding between the adjacent cation complex units and counterbalance chloride ions. The complex showed hysteretic spin-crossover (SCO) behavior above room temperature as evidenced by combined magnetic investigations and differential scanning calorimetry measurements ($T_{1/2} \uparrow = 345$ K, $T_{1/2} \downarrow = 330$ K). In addition, the light-induced excited spin state trapping (LIESST) effect was also observed in the complex. The magnetism-structure relationship shows that the N—H…Cl hydrogen bonding plays an important role in the bistable SCO behavior of the complex. CCDC: 2164316.

Keywords: spin crossover; Fe(III) complex; bistable state; hydrogen bond; supramolecular interactions

收稿日期:2022-04-06。收修改稿日期:2022-09-19。

山西省基础研究计划(自由探索类)项目(No.20210302123355)、山西省高等学校科技创新项目(No.2020L0592)、晋中学院博士基金项目(No.jzxybsjxm2019020)、黄冈师范学院启动基金(No.2042021033)和配位化学国家重点实验室开放基金项目(No.SKLC2208)资助。

*通信联系人。E-mail: shaodong@nju.edu.cn

0 Introduction

The spin crossover (SCO) complex is one of the most attractive molecular materials showing magnetic bistability, which has potential applications in molecular switches, sensors, and display devices^[1-2]. Due to their inherent electronic switching between high-spin (HS) and low-spin (LS), this fascinating physical phenomenon can also be used to control other physical properties via temperature, pressure, light irradiation, or magnetic field^[3]. The most important index for an SCO complex is the performance of its spin transition temperature ($T_{1/2}$) and thermal hysteresis loop width (ΔT). Generally, SCO materials with 30-50 K hysteresis loops centered around room temperature regions are of great importance and widely pursued^[4]. Over the past eight decades, great endeavors have led to many SCO complexes that exhibit various metal centers, molecular structures, and spin bistabilities. However, SCO complexes with room-temperature magnetic bistability are very rare, and the design and construction of high-performance SCO molecules remain challenging^[5-7]. To obtain cooperative SCO property, strong cooperative interactions that act on the SCO metal sites are of great significance, which usually can be achieved through covalent bonding or supramolecular intermolecular interactions, such as hydrogen bonding, π - π interactions, and halogen bonding^[8-12]. Thus, the key development of hysteretic SCO materials is to understand and explore the crystal engineering of efficient supramolecular intermolecular interactions.

Compared with widely studied Fe(II) SCO systems, Fe(III) complexes become more and more attractive because of their higher air stability, which is vital for

practical application^[13-15]. To date, there are several Fe(III) SCO complexes constructed usually by mixed N/O/S coordination donor sets, such as N_4O_2 , N_3O_2S , and $N_2O_2S_2$ ^[13]. In stark comparison, N_6 coordination environments for Fe(III) SCO complexes are very rare. To access N_6 Fe(III) SCO complexes, 2,6-bis(benzimidazol-2-yl)pyridine (bzimpy) is a suitable choice^[16-21]. In fact, this ligand has a fascinating variability in both the chemistry and SCO properties for Fe^{II/III} complexes. Though several bzimpy-based Fe^{II} SCO complexes have been reported, Fe^{III} SCO complexes have not been reported so far^[17-21]. As can be seen in Fig.1, there are two protons in the ligand and thus bzimpy can be deprotonated affording bzimpy-1H and bzimpy-2H. These structural characteristics potentially provide the chance to take advantage of the two protons for the engineering of hydrogen bonding interactions and controlling ligand valence via deprotonation. Considering the high interest in both Fe(III) SCO complexes and supramolecular control on intermolecular interactions, we aim to develop new Fe(III) SCO complexes involving interesting supramolecular interactions.

With the above aspects in mind, a mononuclear Fe(III) complex, $[Fe^{III}(bzimpy-1H)_2]Cl$ (**1**), has been synthesized based on the tridentate chelate ligand bzimpy. Interestingly, the complex is solvent-free and possesses a halogen hydrogen-bonded supramolecular network where the Fe^{3+} center locates in a distorted N_6 octahedral coordination environment. Magnetic measurements indicated that complex **1** exhibited a reversible thermal-induced spin-state switching above room temperature. In addition, a *ca.* 15 K thermal hysteresis loop was observed, suggesting a strong cooperative SCO behavior in **1**.

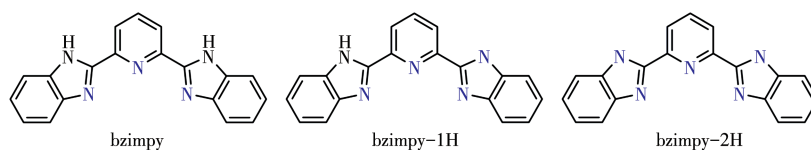


Fig.1 Molecular structures of ligand bzimpy, and its deprotonated species bzimpy-1H and bzimpy-2H

1 Experimental

1.1 Reagents and physical measurements

2,6-Bis(benzimidazol-2-yl)pyridine was directly

purchased from TCI chemicals. Other chemicals were commercially available and used as received without further purification.

The powder X-ray diffraction (PXRD) pattern was

measured by using a Rigaku Smart lab X-ray diffractometer (Cu $K\alpha$ radiation; $\lambda=0.154\ 056\ \text{nm}$; operating current, 30 mA; operating voltage, 40 kV; scanning range, 5° - 35°). Elemental analysis for C, H, and N was performed on an Elemental Vario EL analyzer. The IR spectrum ($4\ 000$ - $400\ \text{cm}^{-1}$) was recorded at room temperature on a Bruker tensor II spectrometer. Thermogravimetric analysis (TGA) was performed by using a Mettler Toledo TGA2 instrument. Differential scanning calorimetry (DSC) was performed using a Mettler Toledo DSC3 apparatus. Variable-temperature direct current (dc) magnetic susceptibility data were gained using a Quantum Design SQUID VSM magnetometer. The photomagnetic experiment was performed on the fresh sample at 10 K by using an irradiation light from a Diode Pumped Solid State laser. All magnetic data were diamagnetically corrected using Pascal's constants. Electron paramagnetic resonance (EPR) studies were performed by using a Bruker E580 X-band electron spin resonance spectrometer operating at 9.4 GHz.

1.2 Synthesis of complex 1

Anhydrous FeCl_3 (0.1 mmol, 16.2 mg) and bzimpy (0.2 mmol, 60 mg) were dissolved in 10 mL acetonitrile giving a dark green mixed solution, which was treated with Et_3N (14.0 μL , 0.1 mmol). The resulting mixture was stirred for a few minutes before filtration. Dark green block crystals were obtained in five days by slow evaporation of the filtrate. Yield 35.8%. Elemental analysis Calcd. for $\text{C}_{38}\text{H}_{24}\text{ClFeN}_{10}$ (%): C, 64.11; H, 3.40; N, 19.67. Found(%): C, 63.92; H, 3.59; N, 19.72. IR (KBr, cm^{-1}): 3 219(s), 2 902(s), 2 767(s), 1 192(s), 1 599(vs), 1 494(s), 1 459(vs), 1 318(s), 1 303(w), 1 217(s), 1 199(w), 1 173(vs), 1 115(vs), 1 028(vs), 1 005(vs), 995(w), 762(w), 690(w), 624(vs), 571(s).

1.3 X-ray crystallography

X-ray single-crystal crystallographic data were collected using a Bruker D8 Quest diffractometer (Mo $K\alpha$ radiation, $\lambda=0.071\ 073\ \text{nm}$). Data collection and structural analysis were performed by the APEX III program. The structure was solved by direct methods and refined by the full-matrix least-squares method on F^2 using the SHELXTL^[22] crystallographic software package integrated into Olex2^[23]. All non-hydrogen

atoms were refined with anisotropic displacement parameters. The crystallographic data and structure refinement parameters for **1** are listed in Table 1.

CCDC: 2164316.

Table 1 Crystallographic data and structure refinement parameters for 1

Parameter	1
Empirical formula	$\text{C}_{38}\text{H}_{24}\text{ClFeN}_{10}$
Formula weight	711.97
Temperature / K	296
Crystal system	Tetragonal
Space group	$P\bar{4}n2$
a / nm	0.994 5(3)
b / nm	0.994 5(3)
c / nm	1.559 8(5)
Volume / nm^3	1.542 7(10)
Z	2
D_c / ($\text{g}\cdot\text{cm}^{-3}$)	1.533
μ / mm^{-1}	0.624
$F(000)$	730.0
$R_{\text{int}}, R_{\sigma}$	0.044 1, 0.035 7
Goodness-of-fit on F^2	1.228
R_1^a, wR_2^b [$I>2\sigma(I)$]	0.059 7, 0.174 4
R_1, wR_2 (all data)	0.062 6, 0.176 5
$(\Delta\rho)_{\text{max}}, (\Delta\rho)_{\text{min}}$ / ($\text{e}\cdot\text{nm}^{-3}$)	530, -370

$$^a R_1 = \sum \|F_o\| - \|F_c\| / \sum \|F_o\|; ^b wR_2 = [\sum w(F_o^2 - F_c^2)^2 / \sum w(F_o^2)^2]^{1/2}.$$

2 Results and discussion

2.1 Crystal structure

The single-crystal X-ray diffraction analysis reveals that complex **1** crystallizes in the tetragonal $P\bar{4}n2$ space group with a discrete mononuclear structure (Fig. 2). One Fe^{3+} center, half one bzimpy-1H anion, and one counter Cl^- ion are found in the asymmetric unit of **1** (Fig. 2a). The complete molecular structure (Fig. 2b) indicates that each Fe^{3+} ion is chelated by six N atoms from two bzimpy-H anion, resulting in a distorted octahedral $[\text{FeN}_6]$ geometry. Notably, the bzimpy ligand should lose one of its protons based on the charge balance. However, it cannot be distinguished in crystallography, leading to a half-occupied H in the bzimpy molecules. To highlight this point, we use bzimpy-1H to clarify the structure. The metal-ligand bond lengths are listed in Table 2. The Fe—

N(im) and Fe—N(py) distances are 0.190 8 and 0.197 8 nm, respectively. The Fe—N(py) distances are significantly larger than the most frequently studied complex [Fe^{II}(bzimpy)₂](ClO₄)₂·0.25H₂O, wherein Fe—N(py) distances are in a range of 0.187 3-0.187 6 nm^[18]. The average Fe—N bond length is 0.195 4 nm, revealing a low spin of Fe³⁺ in **1** at room temperature. Due to the lengths of Fe—N1 and Fe—N1^a being smaller than those of the other Fe—N bonds, the *O_h* geometry is sig-

nificantly compressed. The continuous shape measures (CSM)^[24] value was calculated to be 1.594 (CSM=0 for ideal octahedron), indicating a moderate distortion from *O_h* symmetry. To further detect the structural distortion, OctaDisc software^[25] was used to calculate the distortion parameters, affording that ζ and Σ values were 0.187 275 and 243.023 9, respectively, which was comparable with the reported structurally similar LS Fe³⁺ complexes. As highlighted in Fig.3, interesting-

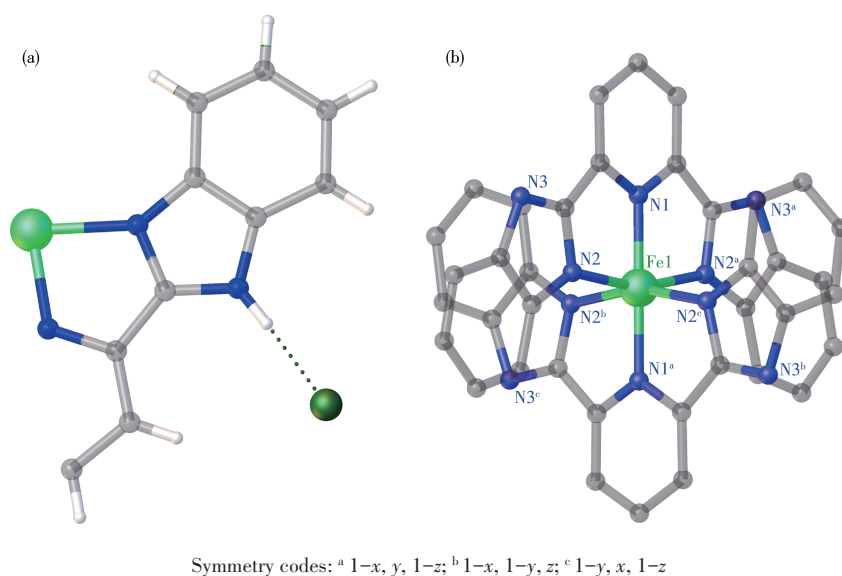


Fig.2 (a) Asymmetric structure unit of **1** with the highlighted Cl···H hydrogen bond; (b) Complete crystal structure of **1**

Table 2 Selected bond lengths (nm) and angles (°) for **1**

Fe1—N1 ^a	0.190 8(10)	Fe1—N2	0.197 8(8)	Fe1—N2 ^b	0.197 8(8)
Fe1—N1	0.190 8(10)	Fe1—N2 ^a	0.197 8(8)	Fe1—N2 ^c	0.197 8(8)
N1 ^a —Fe1—N1	180.0	N1—Fe1—N2 ^b	98.7(2)	N1 ^a —Fe1—N2 ^a	81.3(2)
N2 ^a —Fe1—N2 ^b	162.5(5)	N2 ^c —Fe1—N2 ^a	91.32(7)	N2 ^c —Fe1—N1 ^b	91.32(7)

Symmetry codes: ^a 1-x, y, 1-z; ^b 1-x, 1-y, z; ^c 1-y, x, 1-z.

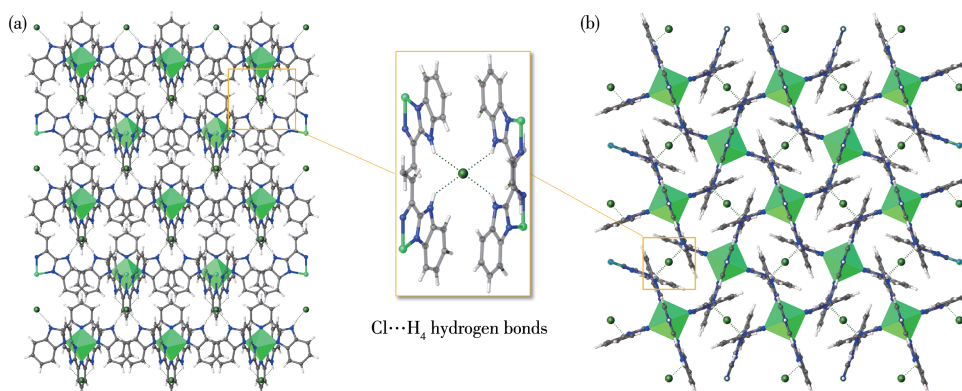


Fig.3 Portion of the packing crystal structure of **1** along with the (100) (a) and (001) (b) direction with a highlight of the Cl···H₄ hydrogen bonds

ly, the mononuclear $[\text{Fe}^{\text{III}}(\text{bzimpy}-1\text{H})_2]^-$ species are connected by Cl^- ions as central connection nodes by forming four $\text{N}-\text{H}\cdots\text{Cl}$ ($\text{Cl}\cdots\text{H}_4$) hydrogen bonds, resulting in a 3D halogen hydrogen-bonded supramolecular network. The distance of the $\text{H}\cdots\text{Cl}$ is 0.217 5 nm while the shortest intermolecular $\text{Fe}\cdots\text{Fe}$ distance is 0.994 5 nm.

2.2 PXRD and TGA

To check the purity of bulk material of **1**, the PXRD experiment was performed. As can be seen in

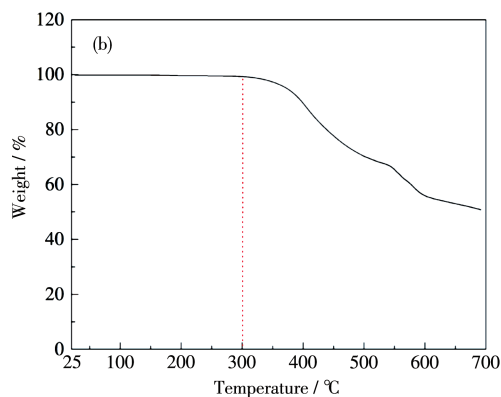
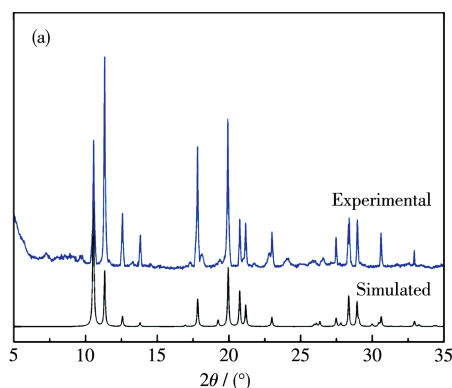


Fig.4 (a) Comparison of the experimental PXRD pattern of **1** with the simulated pattern; (b) TGA curve of **1**

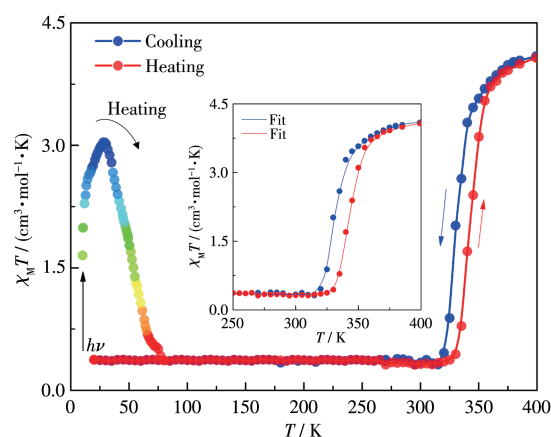
2.3 Magnetic properties

Temperature-dependent magnetic susceptibility was measured on the crystals sample of **1** to investigate the possible SCO behavior (Fig.5). The room temperature $\chi_{\text{M}}T$ value of **1** was $0.41 \text{ cm}^3 \cdot \text{mol}^{-1} \cdot \text{K}$, indicating a low spin Fe^{3+} at this temperature. The $\chi_{\text{M}}T$ value remains nearly constant at 310 K, suggesting a low spin state within this temperature range. However, with the temperature increasing to 330 K, the $\chi_{\text{M}}T$ value abruptly increased to $3.28 \text{ cm}^3 \cdot \text{mol}^{-1} \cdot \text{K}$ at 355 K, and gradually reached $4.09 \text{ cm}^3 \cdot \text{mol}^{-1} \cdot \text{K}$ at 400 K. The subsequent cooling mode indicated that the abrupt decreasing temperature was 340 K and the $\chi_{\text{M}}T$ value reached $0.41 \text{ cm}^3 \cdot \text{mol}^{-1} \cdot \text{K}$ at 325 K. Thus complex **1** exhibited an abrupt hysteretic SCO behavior with $T_{1/2} \uparrow = 345$ and $T_{1/2} \downarrow = 330$ K. The 15 K hysteresis loop indicates significant magnetic bistability for **1**.

Furthermore, to quantitatively detect the cooperativity in **1**, the regular solution model^[26] was used to fit the magnetic susceptibility of **1** with the following equation (1):

$$\ln \frac{(1 - \gamma_{\text{HS}})}{\gamma_{\text{HS}}} = \frac{\Delta H + T(1 - 2\gamma_{\text{HS}})}{RT} - \frac{\Delta S}{R} \quad (1)$$

where γ_{HS} is the molar fraction of HS state; R is the molar gas constant; ΔH and ΔS represent the enthalpy



Inset: fitting of the $\chi_{\text{M}}T$ data by using a regular solution model

Fig.5 Temperature-dependent $\chi_{\text{M}}T$ curves of **1** under 1 kOe dc field, where the solid lines are guided for the eyes, and temperature-dependent $\chi_{\text{M}}T$ measured after irradiation with the 445 nm laser at 10 K

and the entropy variations; Γ is the parameter accounting for cooperativity associated with the spin conversion. The best fits afforded the data for the cooling and heating modes, respectively: $\Delta H = -15.3 \text{ kJ}\cdot\text{mol}^{-1}$, $\Delta S = -59.8 \text{ J}\cdot\text{mol}^{-1}\cdot\text{K}^{-1}$, and $\Gamma = 2.92 \text{ kJ}\cdot\text{mol}^{-1}$; $\Delta H = 16.1 \text{ kJ}\cdot\text{mol}^{-1}$, $\Delta S = 61.2 \text{ J}\cdot\text{mol}^{-1}\cdot\text{K}^{-1}$, and $\Gamma = 2.82 \text{ kJ}\cdot\text{mol}^{-1}$. These fitting parameters are comparable with the reported $\text{Fe}^{2+}/\text{Fe}^{3+}$ SCO complexes. The obtained Γ values were positive and relatively large revealing that the $[\text{Fe}(\text{bzimpy}-1\text{H})_2]^+$ species are liable to be surrounded by molecules of the same spin states to achieve strong cooperativity.

To probe the possible light-induced excited spin state trapping (LIESST) effect of **1**, photomagnetic measurement was also performed. After the sample was irradiated in the SQUID chamber by a 445 nm laser at 10 K, a sharp increase in the magnetization value was observed and the $\chi_M T$ value saturated to $3.03 \text{ cm}^3\cdot\text{mol}^{-1}\cdot\text{K}$ at 28 K after 2 h of irradiation (Fig. 5). This result suggests that the light-induced metastable HS* state is partly trapped by the excitation of Fe^{III} in the LS state. Upon heating, the $\chi_M T$ value dramatically decreased to $0.42 \text{ cm}^3\cdot\text{mol}^{-1}\cdot\text{K}$ at 78 K, indicating a relatively fast relaxation of the metastable HS* state of the Fe^{3+} ions.

2.4 X-band EPR measurement

To further probe the spin state and oxidation state of Fe ion at 300 K, the EPR spectrum was measured. The obtained EPR spectrum is shown in Fig. 6, which exhibits sharp and strong peaks in the vicinity of the 3 000 G field. These EPR signals usually indicate a

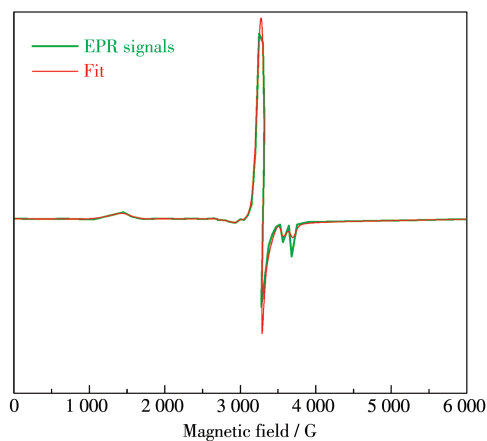


Fig. 6 Solid-state EPR spectrum for complex **1**

triplet-state ($S=1/2$) of the measured complex and are comparable with the characteristic peaks of LS Fe^{III} ^[27-28]. The spectrum was further simulated by the EasySpin-EPR program, giving the anisotropic g -tensors: $g_x=2.20$, $g_y=2.07$, and $g_z=1.94$. These values were typical of those determined for the reported LS Fe^{3+} complexes^[29-30]. Thus, the result is consistent with the crystal data and magnetic measurement.

2.5 DSC measurement

To further probe the SCO transition behavior in **1**, the DSC experiment was performed using a scan rate of $5 \text{ K}\cdot\text{min}^{-1}$ (Fig. 7). As depicted in Fig. 7, a pair of notable sharp exothermic/endothermic peaks could be observed at *ca.* 324 and 340 K during cooling and heating processes, respectively, indicating a hysteretic effect of about 16 K. These results agreed well with the SCO behavior observed in the magnetic measurements. The sharp peaks and thermal hysteretic effect reveal a first-order phase transition happening in **1** during the SCO process. The corresponding enthalpy (ΔH) and entropy (ΔS) values were integrated to be $-11.5/13.1 \text{ kJ}\cdot\text{mol}^{-1}$ and $-50.3/51.7 \text{ J}\cdot\text{mol}^{-1}\cdot\text{K}^{-1}$ for the cooling/heating processes, respectively. These results indicate that the spin transition shows a considerable contribution from the molecular vibrations. The observed values were comparable with the other Fe^{III} SCO complexes with abrupt hysteretic SCO and the fitted results via magnetic susceptibility data.

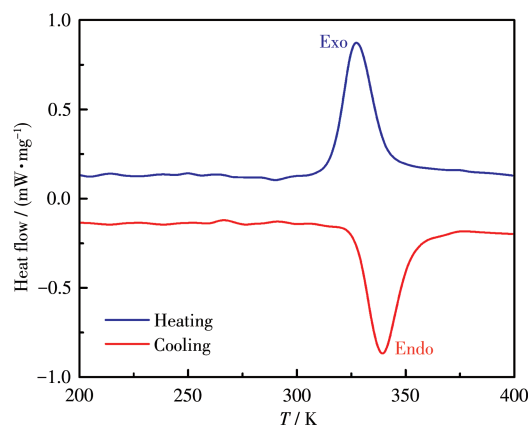


Fig. 7 DSC results of **1** in three cooling and warming cycles with a scan rate of $5 \text{ K}\cdot\text{min}^{-1}$

2.6 Discussion

Based on the studies on Fe^{II} complexes con-

structed by bzimpy, we can conclude that the stoichiometry of the complexes with the content of counter ions and solvates is variable^[17-21]. Their consequences on SCO behavior are significantly affected by supramolecular interactions, including hydrogen bonding networks, π - π stacking interactions, *etc.* These facts can be well illustrated by the $[\text{Fe}^{\text{II}}(\text{bzimpy})_2](\text{ClO}_4)_2 \cdot x\text{H}_2\text{O}$ SCO system. When $x=0.5$, the complex exhibits a 12 K hysteretic SCO with $T_{1/2}=403$ K while no hysteretic SCO with $T_{1/2}=424$ K when $x=2$. Additionally, the counter ions are also critical. For instance, though the complex $[\text{Fe}^{\text{II}}(\text{bzimpy})_2](\text{SO}_4)_2 \cdot 2\text{H}_2\text{O}$ can show SCO behavior, the conversion is far from complete above 500 K. Notably, all the reported bzimpy-based Fe(II) complexes contain lattice solvents. In fact, solvent-free systems are more attractive from the application perspective. The presented complex here is the first example of a bzimpy-based iron complex without solvent. The second distinct characteristic of complex **1** is its counter ions, which is a very simple single ion Cl^- . In comparison, complex **1** is notable among the previously reported relative iron coordination compounds^[16-21].

It has been widely realized that the effective supramolecular interaction in the SCO center is of great importance for cooperative SCO behavior. As two illustrative examples, weber et al. reported a Fe(II) SCO complex showing a 69 K wide thermal hysteresis loop because of the formation of a 2D hydrogen-bonded network^[31]. Hayami and co-workers reported a Fe(III) SCO complex that exhibits very wide thermal hysteresis loops (140 K in the first cycle and 70 K after the first cycle) originating from the 1D network structure induced by π - π interactions between quinoline and phenyl rings^[32]. In the presented complex **1**, the Fe(III) SCO molecules were well bridged by halogen hydrogen bonds via an interesting $\text{Cl}\cdots\text{H}_4$ mode. To the best of our knowledge, such a halogen hydrogen bond is extremely rare^[33]. Thus, we think the halogen hydrogen bonds are a key factor contributing to the strongly cooperative spin transition in **1**. In addition, the high thermal stability is also should be attributed to the halogen hydrogen bonded supramolecular structure. However, the high-temperature structure cannot be measured

due to the drastic spin transition accompanying significant lattice motion, which prevents a detailed study of the structure transformation and lattice vibration during the SCO phase transition.

3 Conclusions

In summary, we describe a mononuclear Fe(III) complex displaying above room-temperature SCO bistability. Single-crystal X-ray diffraction analysis revealed the Fe^{3+} anions are bridged by $\text{N}-\text{H}\cdots\text{Cl}$ hydrogen bonds leading to an interesting halogen hydrogen-bonded supramolecular structure. Magnetic studies indicated that the complex exhibited an abrupt spin transition with a significant 15 K thermal hysteresis loop and LIESST effect. The spin bistability was further established by the DSC experiment. The foregoing results suggest that the introduction of halogen ion and halogen-hydrogen bonding interactions in SCO complexes provides an alternative route for developing strong cooperative SCO materials. Further attempt to design and synthesize more halogen hydrogen-bonded Fe(III) SCO complexes is currently underway in our lab.

References:

- [1] Halcrow M A. *Spin Crossover Materials: Properties and Applications*. New York: Wiley, **2013**.
- [2] Ruben M, Kuppusamy S K. Sublimable Spin-Crossover Complexes: From Spin-State Switching to Molecular Devices. *Angew. Chem. Int. Ed.*, **2021**,**60**(14):7502-7521
- [3] Sato O, Tao J, Zhang Y Z. Control of Magnetic Properties through External Stimuli. *Angew. Chem. Int. Ed.*, **2007**,**46**(13):2152-2187
- [4] Halcrow M A. Structure: Function Relationships in Molecular Spin-Crossover Complexes. *Chem. Soc. Rev.*, **2011**,**40**(7):4119-4142
- [5] Shao D, Shi L, Shen F X, Wei X Q, Sato O, Wang X Y. Reversible On-Off Switching of the Hysteretic Spin Crossover in a Cobalt(II) Complex via Crystal to Crystal Transformation. *Inorg. Chem.*, **2019**,**58**(17): 11589-11598
- [6] Zhao X H, Shao D, Chen J T, Gan D X, Yang J, Zhang Y Z. A Trinuclear $\{\text{Fe}^{\text{III}}_2\text{Fe}^{\text{II}}\}$ Complex Involving Both Spin and Non-spin Transitions Exhibits Three-Step and Wide Thermal Hysteresis. *Sci. China Chem.*, **2022**,**65**(3):532-538
- [7] Shen K Y, Zhang C J, Qu L Y, Jiang S Q, Zhang Y, Tong M L, Bao X. Thermally, Acidity-Driven, and Photo-Driven Spin-State Switching in Pyridylacetylhydrazoniron(II) Complexes at or above Room Temperature. *Inorg. Chem.*, **2021**,**60**(23):18225-18233

- [8] Wang L F, Lv B H, Wu F T, Huang G Z, Ruan Z Y, Chen Y C, Liu M, Ni Z P, Tong M L. Reversible On-Off Switching of Spin-Crossover Behavior via Photochemical [2+2] Cycloaddition Reaction. *Sci. China Chem.*, **2022**,**65**(1):120-127
- [9] Craze A R, Zenno H, Pfrunder M C, McMurtrie J C., Hayami S, Clegg J K, Li F. Supramolecular Modulation of Spin Crossover in an Fe(II) Dinuclear Triple Helicate. *Inorg. Chem.*, **2021**,**60**(9):6731-6738
- [10] Shen F X, Pi Q, Le S, Shao D, Li H Q, Sun Y C. Spin Crossover in Hydrogen-Bonded Frameworks of Fe^{II} Complexes with Organodisulfonate Anions. *Dalton Trans.*, **2019**,**48**(24):8815-8825
- [11] Zhao X H, Zhang S L, Shao D, Wang X Y. Spin Crossover in [Fe(2-picolylamine)₃]²⁺ Adjusted by Organosulfonate Anions. *Inorg. Chem.*, **2015**,**54**(16):7857-7867
- [12] Zhang S L, Zhao X H, Wang Y M, Shao D, Wang X Y. Spin Crossover Behaviour in One-Dimensional Fe^{II} Compounds Based on the [M(CN)₄]²⁻ (M=Pd, Pt) Units. *Dalton Trans.*, **2015**,**44**(20):9682-9690
- [13] Harding D J, Harding P, Phonsri W. Spin Crossover in Iron(III) Complexes. *Coord. Chem. Rev.*, **2016**,**313**:38-61
- [14] Nakaya M, Ohtani R, Lindoy L F, Hayami S. Light-Induced Excited Spin State Trapping in Iron(III) Complexes. *Inorg. Chem. Front.*, **2021**, **8**(2):484-498
- [15] 王康杰, 李鸿庆, 孙宇辰, 王新益. 氢键桥连一维铁(III)自旋交叉化合物的合成和性质. *无机化学学报*, **2020**,**36**(6):1143-1148
WANG K J, LI H Q, SUN Y C, WANG X Y. Synthesis and Properties of an Iron Spin Crossover Compound with 1D Chains Bridged by Hydrogen Bonds. *Chinese J. Inorg. Chem.*, **2020**,**36**(6):1143-1148
- [16] Boca M, Jameson R F, Linert W. Fascinating Variability in the Chemistry and Properties of 2,6-Bis-(benzimidazol-2-yl)-pyridine and 2,6-Bis-(benzthiazol-2-yl)-pyridine and Their Complexes. *Coord. Chem. Rev.*, **2011**,**255**(1/2):290-317
- [17] Ruttimann S, Moreau C M, Williams A F, Bernardinelli G, Addison A W. Complexes of Structural Analogs of Terpyridyl with Iron and Zinc—The X-ray Crystal Structure of Bis[2,6-bis(benzimidazol-2-yl)pyridine]iron (II) Trifluoromethylsulfonate Bis-ethanol Solvate. *Polyhedron*, **1992**,**11**(6):635-646
- [18] Boca R, Baran P, Dlhif L, Fuess H, Haase W, Renz F, Linert W, Svoboda I, Wemer R. Crystal Structure and Spin Crossover Studies on Bis(2,6-bis(benzimidazol-2-yl)pyridine) Iron(II) Perchlorate. *Inorg. Chim. Acta*, **1997**,**260**(2):129-136
- [19] Boca R, Baran P, Boca M, Fuess H, Haase W, Linert W, Papfinkov B, Werner R. Spin Crossover in Bis(2,6-bis(benzimidazol-2-yl)pyridine) Iron(II) Tetrphenylborate. *Inorg. Chim. Acta*, **1998**,**278**(2):190-196
- [20] Boca R, Boca M, Dlhán L, Falk K, Fuess H, Haase W, Jaroščíak R, Papánková B, Renz F, Vrbová M, Werner R. Strong Cooperativeness in the Mononuclear Iron(II) Derivative Exhibiting an Abrupt Spin Transition above 400 K. *Inorg. Chem.*, **2001**,**40**(13):3025-3033
- [21] Boca R, Renz F, Boca M, Fuess H, Haase W, Kicklbick G, Linert W, Vrbova-Schikora M. Tuning the Spin Crossover Above Room Temperature: Iron(II) Complexes of Substituted and Deprotonated 2,6-Bis(benzimidazol-2-yl)pyridine. *Inorg. Chem. Commun.*, **2005**,**8**(2):227-230
- [22] Sheldrick G M. *SHELXTL, Version 6.14*. Bruker AXS, Inc., Madison, WI, **2000-2003**.
- [23] Dolomanov O V, Bourhis L J, Gildea R J, Howard J A K, Puschmann H. OLEX2: A Complete Structure Solution, Refinement and Analysis Program. *J. Appl. Crystallogr.*, **2009**,**42**:339-341
- [24] Llunell M, Casanova D, Cirera J, Alemany P, Alvarez S. *SHAPE, Version 2.1*. University of Barcelona, **2013**.
- [25] Ketkaew R, Tantirungrotechai Y, Harding P, Chastanet G, Guionneau P, Marchivie M, Harding D J. OctaDist: A Tool for Calculating Distortion Parameters in Spin Crossover and Coordination Complexes. *Dalton Trans.*, **2021**,**50**(3):1086-1096
- [26] Martin J P, Zarembowitch J, Bousseksou A, Dworkin A, Haasnoot J G, Varret F. Solid State Effects on Spin Transitions: Magnetic, Calorimetric, and Mössbauer-Effect Properties of [Fe_xCo_{1-x}(4,4'-bis-1,2,4-triazole)₂(NCS)₂] · H₂O Mixed - Crystal Compounds. *Inorg. Chem.*, **1994**,**33**(26):6325-6333
- [27] Domracheva N E, Pyataev A V, Vorobeva V E, Zueva E M. Detailed EPR Study of Spin Crossover Dendrimeric Iron(III) Complex. *J. Phys. Chem. B*, **2013**,**117**(25):7833-7842
- [28] Domracheva N, Pyataev A, Manapov R, Gruzdev M, Chervonova U, Kolker A. Structural, Magnetic and Dynamic Characterization of Liquid Crystalline Iron(III) Schiff Base Complexes with Asymmetric Ligands. *Eur. J. Inorg. Chem.*, **2011**(8):1219-1229
- [29] Thammasangwan W, Harding P, Telfer S G, Alkaş A, Phonsri W, Murray K S, Clérac R, Rouzières M, Chastanet G, Harding D J. Thermal and Light-Activated Spin Crossover in Iron(III) qnal Complexes. *Eur. J. Inorg. Chem.*, **2020**(14):1325-1330
- [30] Ouyang Z J, Mo X Y, Yang M, Zhong L, Chen W B, Gao S, Dong W. High Temperature Fe(III) Spin Crossover Behaviours in Three Unprecedented Fe^{III}—M^{II}—Fe^{III} (M=Fe, Cd) Linear Trinuclear Complexes. *Inorg. Chem. Front.*, **2020**,**7**(7):1526-1531
- [31] Weber B, Bauer W, Obel J. An Iron(II) Spin-Crossover Complex with a 70 K Wide Thermal Hysteresis Loop. *Angew. Chem. Int. Ed.*, **2008**, **47**(52):10098-10101
- [32] Hayami S, Gu Z, Yoshiki H, Fujishima A, Sato O. Iron(III) Spin-Crossover Compounds with a Wide Apparent Thermal Hysteresis around Room Temperature. *J. Am. Chem. Soc.*, **2001**,**123**(47):11644-11650
- [33] Feng L J, Yuan Y H, Yan B J, Feng T T, Jian Y P, Zhang J C, Sun W Y, Lin K, Luo G S, Wang N. Halogen Hydrogen-Bonded Organic Framework (XHOF) Constructed by Singlet Open-Shell Diradical for Efficient Photoreduction of U(VI). *Nat. Commun.*, **2022**,**13**:1389